hep-ex/9709021 v3   7 Oct 1997

Measurement of the Diffractive Structure Function $F_2^{D(4)}$ at HERA

ZEUS Collaboration

Abstract

This paper presents the first analysis of diffractive photon dissociation events in deep inelastic positron-proton scattering at HERA in which the proton in the final state is detected and its momentum measured. The events are selected by requiring a scattered proton in the ZEUS leading proton spectrometer (LPS) with $x_L > 0.97$, where x_L is the fraction of the incoming proton beam momentum carried by the scattered proton. The use of the LPS significantly reduces the contamination from events with diffractive dissociation of the proton into low mass states and allows a direct measurement of t, the square of the four-momentum exchanged at the proton vertex. The dependence of the cross section on t is measured in the interval $0.073 < |t| < 0.4 \text{ GeV}^2$ and is found to be described by an exponential shape with the slope parameter $b = 7.2 \pm 1.1 (\text{stat.})^{+0.7}_{-0.9}(\text{syst.}) \text{ GeV}^{-2}$. The diffractive structure function $F_2^{D(4)}$ is presented as a function of $x_{I\!P} \simeq 1 - x_L$ and β, the momentum fraction of the struck quark with respect to $x_{I\!P}$, and averaged over the t interval $0.073 < |t| < 0.4 \text{ GeV}^2$ and the photon virtuality range $5 < Q^2 < 20 \text{ GeV}^2$. In the kinematic range $4 \times 10^{-4} < x_{I\!P} < 0.03$ and $0.015 < \beta < 0.5$, the $x_{I\!P}$ dependence of $F_2^{D(4)}$ is fitted with a form $(1/x_{I\!P})^a$, yielding $a = 1.00 \pm 0.09 \text{ (stat.)}^{+0.11}_{-0.05}(\text{syst.})$. Upon integration over t, the structure function $F_2^{D(3)}$ is determined in a kinematic range extending to higher $x_{I\!P}$ and lower β compared to our previous analysis; the results are discussed within the framework of Regge theory.

The ZEUS Collaboration

J. Breitweg, M. Derrick, D. Krakauer, S. Magill, D. Mikunas, B. Musgrave, J. Repond, R. Stanek, R.L. Talaga, R. Yoshida, H. Zhang
Argonne National Laboratory, Argonne, IL, USA [p]

M.C.K. Mattingly
Andrews University, Berrien Springs, MI, USA

F. Anselmo, P. Antonioli, G. Bari, M. Basile, L. Bellagamba, D. Boscherini, A. Bruni, G. Bruni, G. Cara Romeo, G. Castellini[1], M. Chiarini, L. Cifarelli[2], F. Cindolo, A. Contin, M. Corradi, S. De Pasquale, I. Gialas[3], P. Giusti, G. Iacobucci, G. Laurenti, G. Levi, A. Margotti, T. Massam, R. Nania, C. Nemoz, F. Palmonari, A. Pesci, A. Polini, F. Ricci, G. Sartorelli, Y. Zamora Garcia[4], A. Zichichi
University and INFN Bologna, Bologna, Italy [f]

C. Amelung, A. Bornheim, I. Brock, K. Coböken, J. Crittenden, R. Deffner, M. Eckert, M. Grothe, H. Hartmann, K. Heinloth, L. Heinz, E. Hilger, H.-P. Jakob, U.F. Katz, R. Kerger, E. Paul, M. Pfeiffer, Ch. Rembser[5], J. Stamm, R. Wedemeyer[6], H. Wieber
Physikalisches Institut der Universität Bonn, Bonn, Germany [c]

D.S. Bailey, S. Campbell-Robson, W.N. Cottingham, B. Foster, R. Hall-Wilton, M.E. Hayes, G.P. Heath, H.F. Heath, J.D. McFall, D. Piccioni, D.G. Roff, R.J. Tapper
H.H. Wills Physics Laboratory, University of Bristol, Bristol, U.K. [o]

M. Arneodo[7], R. Ayad, M. Capua, A. Garfagnini, L. Iannotti, M. Schioppa, G. Susinno
Calabria University, Physics Dept.and INFN, Cosenza, Italy [f]

J.Y. Kim, J.H. Lee, I.T. Lim, M.Y. Pac[8]
Chonnam National University, Kwangju, Korea [h]

A. Caldwell[9], N. Cartiglia, Z. Jing, W. Liu, B. Mellado, J.A. Parsons, S. Ritz[10], S. Sampson, F. Sciulli, P.B. Straub, Q. Zhu
Columbia University, Nevis Labs., Irvington on Hudson, N.Y., USA [q]

P. Borzemski, J. Chwastowski, A. Eskreys, J. Figiel, K. Klimek, M.B. Przybycień, L. Zawiejski
Inst. of Nuclear Physics, Cracow, Poland [j]

L. Adamczyk[11], B. Bednarek, M. Bukowy, K. Jeleń, D. Kisielewska, T. Kowalski, M. Przybycień, E. Rulikowska-Zarębska, L. Suszycki, J. Zając
Faculty of Physics and Nuclear Techniques, Academy of Mining and Metallurgy, Cracow, Poland [j]

Z. Duliński, A. Kotański
Jagellonian Univ., Dept. of Physics, Cracow, Poland [k]

G. Abbiendi[12], L.A.T. Bauerdick, U. Behrens, H. Beier, J.K. Bienlein, G. Cases[13], O. Deppe, K. Desler, G. Drews, U. Fricke, D.J. Gilkinson, C. Glasman, P. Göttlicher, T. Haas, W. Hain, D. Hasell, K.F. Johnson[14], M. Kasemann, W. Koch, U. Kötz, H. Kowalski, J. Labs, L. Lindemann, B. Löhr, M. Löwe[15], O. Mańczak, J. Milewski, T. Monteiro[16], J.S.T. Ng[17], D. Notz, K. Ohrenberg[18], I.H. Park[19], A. Pellegrino, F. Pelucchi, K. Piotrzkowski, M. Roco[20], M. Rohde, J. Roldán, J.J. Ryan, A.A. Savin, U. Schneekloth, F. Selonke, B. Surrow, E. Tassi, T. Voß[21], D. Westphal, G. Wolf, U. Wollmer[22], C. Youngman, A.F. Żarnecki, W. Zeuner
Deutsches Elektronen-Synchrotron DESY, Hamburg, Germany

B.D. Burow, H.J. Grabosch, A. Meyer, S. Schlenstedt
DESY-IfH Zeuthen, Zeuthen, Germany

G. Barbagli, E. Gallo, P. Pelfer
University and INFN, Florence, Italy [f]

G. Anzivino, G. Maccarrone, L. Votano
INFN, Laboratori Nazionali di Frascati, Frascati, Italy [f]

A. Bamberger, S. Eisenhardt, P. Markun, T. Trefzger[23], S. Wölfle
Fakultät für Physik der Universität Freiburg i.Br., Freiburg i.Br., Germany [c]

J.T. Bromley, N.H. Brook, P.J. Bussey, A.T. Doyle, N. Macdonald, D.H. Saxon, L.E. Sinclair, E. Strickland, R. Waugh
Dept. of Physics and Astronomy, University of Glasgow, Glasgow, U.K. [o]

I. Bohnet, N. Gendner, U. Holm, A. Meyer-Larsen, H. Salehi, K. Wick
Hamburg University, I. Institute of Exp. Physics, Hamburg, Germany [c]

L.K. Gladilin[24], D. Horstmann, D. Kçira, R. Klanner, E. Lohrmann, G. Poelz, W. Schott[25], F. Zetsche
Hamburg University, II. Institute of Exp. Physics, Hamburg, Germany [c]

T.C. Bacon, I. Butterworth, J.E. Cole, G. Howell, B.H.Y. Hung, L. Lamberti[26], K.R. Long, D.B. Miller, N. Pavel, A. Prinias[27], J.K. Sedgbeer, D. Sideris
Imperial College London, High Energy Nuclear Physics Group, London, U.K. [o]

U. Mallik, S.M. Wang, J.T. Wu
University of Iowa, Physics and Astronomy Dept., Iowa City, USA [p]

P. Cloth, D. Filges
Forschungszentrum Jülich, Institut für Kernphysik, Jülich, Germany

J.I. Fleck[5], T. Ishii, M. Kuze, I. Suzuki[28], K. Tokushuku, S. Yamada, K. Yamauchi, Y. Yamazaki[29]
Institute of Particle and Nuclear Studies, KEK, Tsukuba, Japan [g]

S.J. Hong, S.B. Lee, S.W. Nam[30], S.K. Park
Korea University, Seoul, Korea [h]

F. Barreiro, J.P. Fernández, G. García, R. Graciani, J.M. Hernández, L. Hervás[5], L. Labarga, M. Martínez, J. del Peso, J. Puga, J. Terrón[31], J.F. de Trocóniz
Univer. Autónoma Madrid, Depto de Física Teórica, Madrid, Spain [n]

F. Corriveau, D.S. Hanna, J. Hartmann, L.W. Hung, W.N. Murray, A. Ochs, M. Riveline, D.G. Stairs, M. St-Laurent, R. Ullmann
McGill University, Dept. of Physics, Montréal, Québec, Canada [a], [b]

T. Tsurugai
Meiji Gakuin University, Faculty of General Education, Yokohama, Japan

V. Bashkirov, B.A. Dolgoshein, A. Stifutkin
Moscow Engineering Physics Institute, Moscow, Russia [l]

G.L. Bashindzhagyan, P.F. Ermolov, Yu.A. Golubkov, L.A. Khein, N.A. Korotkova, I.A. Korzhavina, V.A. Kuzmin, O.Yu. Lukina, A.S. Proskuryakov, L.M. Shcheglova[32], A.N. Solomin[32], S.A. Zotkin
Moscow State University, Institute of Nuclear Physics, Moscow, Russia [m]

C. Bokel, M. Botje, N. Brümmer, F. Chlebana[20], J. Engelen, E. Koffeman, P. Kooijman, A. van Sighem, H. Tiecke, N. Tuning, W. Verkerke, J. Vossebeld, M. Vreeswijk[5], L. Wiggers, E. de Wolf
NIKHEF and University of Amsterdam, Amsterdam, Netherlands [i]

D. Acosta, B. Bylsma, L.S. Durkin, J. Gilmore, C.M. Ginsburg, C.L. Kim, T.Y. Ling, P. Nylander, T.A. Romanowski[33]
Ohio State University, Physics Department, Columbus, Ohio, USA [p]

H.E. Blaikley, R.J. Cashmore, A.M. Cooper-Sarkar, R.C.E. Devenish, J.K. Edmonds, J. Große-Knetter[34], N. Harnew, M. Lancaster[35], C. Nath, V.A. Noyes[27], A. Quadt, O. Ruske, J.R. Tickner, H. Uijterwaal, R. Walczak, D.S. Waters
Department of Physics, University of Oxford, Oxford, U.K. [o]

A. Bertolin, R. Brugnera, R. Carlin, F. Dal Corso, U. Dosselli, S. Limentani, M. Morandin, M. Posocco, L. Stanco, R. Stroili, C. Voci
Dipartimento di Fisica dell' Università and INFN, Padova, Italy [f]

J. Bulmahn, B.Y. Oh, J.R. Okrasiński, W.S. Toothacker, J.J. Whitmore
Pennsylvania State University, Dept. of Physics, University Park, PA, USA [q]

Y. Iga
Polytechnic University, Sagamihara, Japan [g]

G. D'Agostini, G. Marini, A. Nigro, M. Raso
Dipartimento di Fisica, Univ. 'La Sapienza' and INFN, Rome, Italy [f]

J.C. Hart, N.A. McCubbin, T.P. Shah
Rutherford Appleton Laboratory, Chilton, Didcot, Oxon, U.K. [o]

E. Barberis[35], D. Epperson, C. Heusch, J.T. Rahn, H.F.-W. Sadrozinski, A. Seiden, R. Wichmann, D.C. Williams
University of California, Santa Cruz, CA, USA [p]

O. Schwarzer, A.H. Walenta
Fachbereich Physik der Universität-Gesamthochschule Siegen, Germany [c]

IV

H. Abramowicz[36], G. Briskin, S. Dagan[36], S. Kananov[36], A. Levy[36]
Raymond and Beverly Sackler Faculty of Exact Sciences, School of Physics, Tel-Aviv University, Tel-Aviv, Israel [e]

T. Abe, T. Fusayasu, M. Inuzuka, K. Nagano, K. Umemori, T. Yamashita
Department of Physics, University of Tokyo, Tokyo, Japan [g]

R. Hamatsu, T. Hirose, K. Homma[37], S. Kitamura[38], T. Matsushita
Tokyo Metropolitan University, Dept. of Physics, Tokyo, Japan [g]

R. Cirio, M. Costa, M.I. Ferrero, S. Maselli, V. Monaco, C. Peroni, M.C. Petrucci, M. Ruspa, R. Sacchi, A. Solano, A. Staiano
Università di Torino, Dipartimento di Fisica Sperimentale and INFN, Torino, Italy [f]

M. Dardo
II Faculty of Sciences, Torino University and INFN - Alessandria, Italy [f]

D.C. Bailey, C.-P. Fagerstroem, R. Galea, G.F. Hartner, K.K. Joo, G.M. Levman, J.F. Martin, R.S. Orr, S. Polenz, A. Sabetfakhri, D. Simmons, R.J. Teuscher[5]
University of Toronto, Dept. of Physics, Toronto, Ont., Canada [a]

J.M. Butterworth, C.D. Catterall, T.W. Jones, J.B. Lane, R.L. Saunders, J. Shulman, M.R. Sutton, M. Wing
University College London, Physics and Astronomy Dept., London, U.K. [o]

J. Ciborowski, G. Grzelak[39], M. Kasprzak, K. Muchorowski[40], R.J. Nowak, J.M. Pawlak, R. Pawlak, T. Tymieniecka, A.K. Wróblewski, J.A. Zakrzewski
Warsaw University, Institute of Experimental Physics, Warsaw, Poland [j]

M. Adamus
Institute for Nuclear Studies, Warsaw, Poland [j]

C. Coldewey, Y. Eisenberg[36], D. Hochman, U. Karshon[36]
Weizmann Institute, Department of Particle Physics, Rehovot, Israel [d]

W.F. Badgett, D. Chapin, R. Cross, S. Dasu, C. Foudas, R.J. Loveless, S. Mattingly, D.D. Reeder, W.H. Smith, A. Vaiciulis, M. Wodarczyk
University of Wisconsin, Dept. of Physics, Madison, WI, USA [p]

S. Bhadra, W.R. Frisken, M. Khakzad, W.B. Schmidke
York University, Dept. of Physics, North York, Ont., Canada [a]

V

1 Introduction

A distinct class of events in deep inelastic neutral current positron-proton scattering (DIS) is experimentally characterized by the proton emerging intact (or excited into a low-mass state) and well separated in rapidity from the state produced by the dissociation of the virtual photon [1, 2]. These large rapidity gap events can be interpreted as being due to diffractive interactions mediated by the exchange of a colourless object with the vacuum quantum numbers, generically called the pomeron.

In diffractive single dissociation DIS events at HERA, $ep \to eXp$, the virtual photon dissociates into a hadronic system of mass M_X, while the proton remains intact; for small $|t|$ ($|t| \lesssim 1$ GeV^2), where t is the square of the four-momentum transfer at the proton vertex, the scattered proton escapes through the beam pipe without being detected in the central apparatus. Therefore diffractive interactions have been studied so far in the H1 and ZEUS experiments either by requiring a large rapidity gap [3, 4, 5] or exploiting the different behaviour of the $\ln(M_X^2)$ distribution for diffractive and non-diffractive events [6]. In both approaches, in the ZEUS results, the hadronic mass M_X was limited to values below 20 GeV.

This paper presents the first analysis of diffractive DIS events in which the proton in the final state is detected and its momentum is measured. The measurement was performed with the ZEUS detector at HERA, using the leading proton spectrometer (LPS) which detects the scattered proton at small angles ($\lesssim 1$ mrad) with respect to the incoming proton beam and measures its momentum. The events were selected by requiring that the scattered proton carry a fraction of the incident proton beam momentum, x_L, greater than 0.97, a region where pomeron exchange dominates. The use of the LPS allows a direct measurement of t, and extends the measurement to higher values of M_X than in our previous analyses.

2 The diffractive structure function $F_2^{D(4)}$

The dependence of the total hadron-hadron and photon-hadron cross sections on the centre of mass (c.m.) energy is related in the Regge approach to the pomeron trajectory. A fit to the hadron-hadron data [7] yielded a universal pomeron trajectory $\alpha_{I\!P}(t) = \alpha_{I\!P}(0) + \alpha'_{I\!P} t$, with $\alpha_{I\!P}(0) \simeq 1.08$ (the 'soft' pomeron). The dependence of the elastic hadron-hadron cross section on t is well described by an exponential distribution at small $|t|$, with a slope that increases with the c.m. energy (shrinkage), leading to $\alpha'_{I\!P} \simeq 0.25$ GeV^{-2}. Regge theory can also be used to describe inclusive diffractive dissociation [8]. These processes have been studied in hadron-hadron (see e.g. [9]-[13]), photon-hadron ([14]-[16]) and DIS ([3]-[6]) interactions.

For diffractive single dissociation in DIS, $e^+(k)p(P) \to e^+(k')Xp(P')$, the cross section can be expressed in terms of the diffractive structure function $F_2^{D(4)}$:

$$\frac{d^4\sigma_{diff}}{d\beta dQ^2 dx_{I\!P} dt} = \frac{2\pi\alpha^2}{\beta Q^4}\left(1 + (1-y)^2\right) F_2^{D(4)}(\beta, Q^2, x_{I\!P}, t), \tag{1}$$

where α is the electromagnetic coupling constant and the contributions of the longitudinal structure function and of Z^0 exchange have been neglected. Note that, with this definition, $F_2^{D(4)}$ has dimensions of GeV^{-2}. Integrating over t, we can define a structure function $F_2^{D(3)}$:

$$\frac{d^3\sigma_{diff}}{d\beta dQ^2 dx_{I\!P}} = \frac{2\pi\alpha^2}{\beta Q^4}\left(1+(1-y)^2\right)F_2^{D(3)}(\beta, Q^2, x_{I\!P}). \tag{2}$$

The relevant kinematic variables are defined as follows. Deep inelastic scattering events are described by $Q^2 = -q^2 = -(k-k')^2$, the negative of the squared four-momentum transfer carried by the virtual photon; by the Bjorken variable $x = \frac{Q^2}{2P\cdot q}$; and by $y = Q^2/xs$, the fractional energy transferred to the proton in its rest frame, where $\sqrt{s} = 300$ GeV is the ep c.m. energy. The c.m. energy of the virtual photon-proton (γ^*p) system is $W \simeq \sqrt{Q^2(1/x-1)}$.

Additional variables are required to describe diffractive scattering:

$$t = (P-P')^2, \quad x_{I\!P} = \frac{(P-P')\cdot q}{P\cdot q}, \quad \beta = \frac{Q^2}{2(P-P')\cdot q} = \frac{x}{x_{I\!P}}, \tag{3}$$

where $x_{I\!P}$ is the momentum fraction of the proton carried by the pomeron. In models where the pomeron has a partonic structure (see e.g. [17]), β is the momentum fraction of the struck quark within the pomeron.

Assuming factorization, as in the model of Ingelman and Schlein [17], the structure function $F_2^{D(4)}$ is factorized into a pomeron flux, depending on $x_{I\!P}$ and t, and a pomeron structure function, which depends on β and Q^2:

$$F_2^{D(4)} = f_{I\!P}(x_{I\!P}, t) \cdot F_2^{I\!P}(\beta, Q^2). \tag{4}$$

In Regge theory the $x_{I\!P}$ dependence of the flux can be expressed as $(1/x_{I\!P})^{2\alpha_{I\!P}(t)-1}$.

In this paper, we present a measurement of the structure function $F_2^{D(4)}$ in the process $ep \to eXp$ in the range $0.015 < \beta < 0.5$, $4 \times 10^{-4} < x_{I\!P} < 0.03$ and averaged over Q^2 between 5 and 20 GeV^2 and over t in the interval $0.073 < |t| < 0.4$ GeV^2. We also present a measurement of the differential cross section as a function of t in a similar kinematic range.

3   Experimental setup

3.1   HERA

In 1994 HERA operated with 153 colliding bunches of $E_p = 820$ GeV protons and $E_e = 27.5$ GeV positrons. Additionally 15 unpaired positron and 17 unpaired proton bunches circulated and were used to determine beam related background. The integrated luminosity for the present study, which required the leading proton spectrometer to be in operating position (see below), is 900 ± 14 nb^{-1}.

3.2 The ZEUS detector

A detailed description of the ZEUS detector is given elsewhere [18]. The main components of the detector used in this analysis are the uranium-scintillator calorimeter, the tracking detectors and the leading proton spectrometer.

The uranium-scintillator calorimeter (CAL) covers 99.7% of the solid angle and is divided into three parts, the forward[1] (FCAL, covering the range $4.3 > \eta > 1.1$ in pseudorapidity), the barrel (BCAL, $1.1 > \eta > -0.75$) and the rear (RCAL, $-0.75 > \eta > -3.8$). Each part is longitudinally subdivided into electromagnetic (EMC) and hadronic (HAC) sections with typical cell sizes of 5×20 cm^2 in the EMC (10×20 cm^2 in the RCAL) and 20×20 cm^2 in the HAC. The timing resolution is better than 1 ns for energy deposits greater than 4 GeV. The energy resolution was measured in test beams [19] to be $\sigma/E = 18\%/\sqrt{E}$(GeV) for electrons and $\sigma/E = 35\%/\sqrt{E}$(GeV) for hadrons. In order to minimize the effects of noise due to the uranium activity, the isolated EMC (HAC) cells with energy less than 100 (150) MeV were discarded from the analysis.

The tracking system consists of two concentric cylindrical drift chambers, the vertex detector (VXD) [20] and the central tracking detector (CTD) [21], operating in a magnetic field of 1.43 T. The CTD, which encloses the VXD, is a drift chamber consisting of 72 cylindrical layers, arranged in 9 superlayers. The measured resolution in transverse momentum for tracks with hits in all superlayers is $\sigma_{p_T}/p_T = 0.005p_T \oplus 0.016$ (p_T in GeV). The interaction vertex is measured with a resolution of 0.4 cm in Z and 0.1 cm in the XY plane.

The position of the scattered positron close to the rear beam pipe region is determined with precision by the small-angle rear tracking detector (SRTD), consisting of 2 planes of scintillator strips attached to the front face of the RCAL, covering an area of 68×68 cm^2. A hole of 20×20 cm^2 at the centre of the RCAL and the SRTD accommodates the beam pipe. The SRTD signals resolve single minimum ionizing particles and provide a position resolution of 0.3 cm. The time resolution is better than 2 ns for a minimum ionizing particle. The SRTD is also used as a presampler to correct the positron energy for losses in the inactive material in front of the rear calorimeter [22].

The proton remnant tagger (PRT1) [16] is a set of scintillator counters surrounding the beam pipe in the forward part of the ZEUS detector at $Z = 5$ m. The tagger consists of two layers of scintillating materials separated by a 1 mm thick lead absorber. Each layer is split vertically into two halves and each half is read out by a photomultiplier tube. The geometric acceptance of PRT1 extends over the pseudorapidity region $4.2 < \eta < 5.8$.

The luminosity is determined via the bremsstrahlung process $e^+p \rightarrow e^+p\gamma$ by measuring energetic photons in a lead-scintillator calorimeter (LUMI) placed at $Z = -107$ m along the beam line [23].

The LPS [24] measures protons scattered at very small angles with respect to the beam line and escaping the central apparatus through the forward beam hole. Such protons carry a substantial

---

[1]The ZEUS coordinate system is right-handed with the Z-axis pointing in the proton beam direction, referred to as forward, and the X-axis horizontal pointing towards the centre of HERA. The pseudorapidity η is defined as $-\ln(\tan\frac{\theta}{2})$, where the polar angle θ is measured with respect to the proton beam direction.

fraction x_L of the incoming proton momentum and have a small transverse momentum p_T ($\lesssim 1$ GeV). The spectrometer consists of six detector stations located at distances of 23 to 90 m along the proton beam line. In 1994 the three most forward stations S4, S5 and S6 were operational: each of these stations consists of an upper and a lower half, which partially overlap during data-taking. Each half is equipped with six rectangular parallel planes of silicon micro-strip detectors. Three different strip orientations (two vertical, two at $+45°$ with respect to the vertical direction and two at $-45°$) are used, in order to remove reconstruction ambiguities. The dimensions of the planes vary from station to station and are approximately 4×6 cm^2; the pitch is 115 μm for the planes with vertical strips and 81 μm for the other planes. The edges of the detectors closest to the beam have an elliptical contour which follows the 10σ profile of the beam, where σ is the standard deviation of the beam spatial distribution in the transverse plane. During data-taking, the planes are inserted in the beam pipe by means of re-entrant Roman pots [25] and are retracted during beam dump and filling operations of the HERA machine. The LPS coordinates are reconstructed with a precision of approximately 35 μm, which includes the intrinsic resolution of the coordinate reconstruction and the alignment precision of the detector stations. The track deflection induced by the magnets in the proton beam line is used for momentum analysis of the scattered proton. The x_L resolution was determined using elastic ρ^0 photoproduction events to be better than 0.4% at 820 GeV; the intrinsic p_T resolution is approximately 5 MeV at $x_L = 1$ and is less than the spread introduced by the angular divergence of the proton beam (which is 40 MeV in the horizontal and 90 MeV in the vertical plane).

4   Reconstruction of kinematic variables

In order to reconstruct the kinematic variables x, Q^2 and W (see section 2), the so-called "Double Angle" method [26] was used, which derives the above quantities from the scattering angle of the positron and that of the struck (massless) quark. The latter is deduced from the momenta of all final state particles, except the scattered proton and positron.

The final state particles in the reaction $e^+ p \to e^+ X p$ were reconstructed from the tracks and calorimeter energy deposits. The scattered positron identification algorithm was based on a neural network [27] which uses information from the CAL. The momenta of the particles of the system X were reconstructed from calorimeter clusters and from tracks in the CTD. The calorimeter clusters were formed by grouping CAL cells into cones around the cell with a local energy maximum. The position of these objects was given by the sum of the positions of the single cells weighted by the logarithm of their energy. Reconstructed tracks were required to have transverse momenta of at least 100 MeV and were matched to clusters with a procedure based on the distance of closest approach. In case the cluster (track) was not matched to a track (cluster), the momentum of the particle was reconstructed only from the cluster (track). When the calorimeter cluster was matched to a track, the track momentum measurement was taken if the following two conditions were satisfied: the ratio between the energy of the cluster and the track momentum was less than 0.8; the track momentum resolution was better than the calorimeter energy resolution. If these two criteria were not satisfied, the particle momentum was reconstructed from the calorimeter cluster energy. An appropriate algorithm was developed for the cases in which more tracks pointed to a single cluster or more clusters were matched

to one track. The use of tracks improves the M_X resolution and reduces the sensitivity to the losses due to inactive material in front of the calorimeter.

The quantity t was determined from the fractional momentum $x_L = p^{LPS}/E_p \simeq p_Z^{LPS}/E_p$ of the scattered proton measured in the LPS and its transverse momentum p_T^{LPS} with respect to the proton beam direction:

$$t = -\frac{(p_T^{LPS})^2}{x_L}. \tag{5}$$

The t resolution is approximately $\sigma(|t|) = 140$ MeV$\sqrt{|t|}$ (t in GeV^2) and is dominated by the angular beam spread.

The quantities $x_{I\!P}$ and β were reconstructed using the values of Q^2 and W^2 determined with the double angle method and the mass of the final hadronic system M_X:

$$x_{I\!P} = \frac{M_X^2 + Q^2}{W^2 + Q^2}, \quad \beta = \frac{Q^2}{Q^2 + M_X^2}. \tag{6}$$

The mass M_X was measured in two ways. In the first method, it was reconstructed as:

$$(M_X^{meas})^2 = (\sum_h E^h)^2 - (\sum_h p_X^h)^2 - (\sum_h p_Y^h)^2 - (\sum_h p_Z^h)^2, \tag{7}$$

where the sums run over all particles detected, except the scattered positron and proton, and $\vec{p}^{\,h} = (p_X^h, p_Y^h, p_Z^h)$ is the momentum vector assigned to each particle of energy E^h. From Monte Carlo studies the resolution on M_X^{meas} was found to be approximately 40% for $M_X^{meas} < 3$ GeV, 18% in the range between 3 and 10 GeV and 14% for M_X^{meas} between 10 and 30 GeV. The mean reconstructed M_X^{meas} is 80% of its true value for all values of M_X^{meas}: therefore an overall correction factor of 1.25 was applied. In the second method, M_X was reconstructed using the LPS and the double angle variables:

$$(M_X^{LPS})^2 = (1 - x_L)(W^2 + Q^2 - m_p^2) - Q^2 + t, \tag{8}$$

where m_p is the proton mass. When x_L approaches unity (low M_X), the resolution on M_X^{LPS} worsens. Monte Carlo studies showed a resolution of 17% for $M_X^{LPS} > 10$ GeV, of 35% for M_X^{LPS} between 3 and 10 GeV and a substantially worse resolution for $M_X^{LPS} < 3$ GeV. No additional correction factor was needed.

In the analysis described here, the first reconstruction method was used to evaluate the mass M_X, calculated as $1.25 \cdot M_X^{meas}$: the resulting resolutions on $x_{I\!P}$ and β in the measured range are 30% and 25%, respectively. A mixed method with M_X^{LPS} for high masses was used as a systematic check.

5 Monte Carlo simulation and LPS acceptance

The diffractive single dissociation process, $e^+ p \to e^+ X p$, was modelled using two Monte Carlo (MC) generators which assume pomeron exchange, the RAPGAP program and a program based

on the Nikolaev and Zakharov model, as well as a MC generator for the exclusive reaction $e^+p \rightarrow e^+\rho^0 p$.

The RAPGAP [28] program is based on a factorizable model [17] in which the incoming proton emits a pomeron, whose constituents take part in the hard scattering. For the pomeron flux, the Streng parametrization [29] was used, which has an effective t dependence ranging from $e^{-5|t|}$ to $e^{-9|t|}$ in the $x_{I\!P}$ range covered by the present measurement; for the pomeron structure function the form fitted in our previous analysis [4] was taken, which contains a mixture of a "hard" ($\propto \beta(1-\beta)$) and a "soft" ($\propto (1-\beta)^2$) quark parton density, with no Q^2 evolution. The program is interfaced to HERACLES [30] for the QED radiative corrections, the parton shower is simulated using the colour-dipole model as implemented in ARIADNE [31] and the fragmentation is carried out with the Lund string model as in JETSET [32]. The region of low masses was tuned to the measured ratio of ϕ to ρ^0 resonance production [33]. The events were generated with a lower x_L cut of 0.9 and with $|t| < 1$ GeV^2.

The Nikolaev and Zakharov model pictures the diffractive dissociation of the photon as a fluctuation of the photon into a $q\bar{q}$ or $q\bar{q}g$ state [34]. The interaction with the proton proceeds via the exchange of a two-gluon colour-singlet state. The cross section can be approximated in terms of a two-component structure function of the pomeron, each with its own flux factor. The hard component, corresponding to the $q\bar{q}$ state, has a β dependence of the form $\beta(1-\beta)$ and an exponential t distribution with a slope of approximately 10 GeV^{-2}. The soft component, which corresponds to the $q\bar{q}g$ state, has a β dependence of the form $(1-\beta)^2$ and a t slope of about 6 GeV^{-2}. In the Monte Carlo implementation of this model [35], hereafter referred to as NZ, the mass spectrum contains both components but the $q\bar{q}g$ states are fragmented (using JETSET) into hadrons as if they were a $q\bar{q}$ system with the same mass. The generation is limited to $M_X > 1.7$ GeV.

To improve the description of the low mass region, events in the region $M_X < 1.7$ GeV were generated separately using a MC for exclusive ρ^0 electroproduction, $ep \rightarrow e\rho^0 p$. In this MC the total cross section for the process $\gamma^*p \rightarrow \rho^0 p$ and the ratio of the longitudinal to the transverse cross section are derived from a parametrization of ZEUS [36] and low energy data. The generator is interfaced to HERACLES which simulates the initial and final state radiation. The RAPGAP sample and the ρ^0 MC sample were mixed in such a way that the weighted sum reproduced the observed M_X distribution in the data: only a small contribution from the ρ^0 MC needed to be added and this mixture was used for the acceptance correction. In a similar way, the NZ and the ρ^0 MC were mixed and used as a systematic check.

In order to estimate the background, the following processes were generated. The events where the proton dissociates into a state of mass M_N ($ep \rightarrow eXN$) were generated with the EPSOFT [37] and PYTHIA [38] programs, where the mass spectrum of the nucleon system and the ratio of double to single dissociation are generated according to measurements from proton-proton colliders [9]. The M_N^2 spectrum is of the form $1/M_N^\alpha$, with $\alpha \simeq 2$. To evaluate the background due to the one-pion exchange process, the RAPGAP MC implementation of this exchange was used, in which the flux of pions is assumed to be $f_\pi(x_\pi, t) \simeq (1 - 4m_\pi^2)^2/(1 - 4t)^2 \cdot (x_\pi t/(t - m_\pi^2)^2)$ [39], where m_π denotes the pion mass and x_π is the fraction of the proton momentum carried by the pion.

All generated events were passed through the standard ZEUS detector simulation, based on the GEANT program [40], and through the trigger simulation and the event reconstruction package. For the scattered proton the simulation includes the geometry of the beam pipe apertures, the HERA magnets and their fields, and the response and noise of the LPS detectors. An accurate simulation of the interaction vertex position and of the effect of the proton beam tilt and emittance is also included.

The distribution of the detected proton transverse momentum, p_T^{LPS}, is limited by the geometric acceptance of the LPS, which depends on the geometry of the beam pipe and the elliptical cutouts in the silicon detector planes. Figure 1 shows the LPS geometric acceptance for tracks with $x_L = 1$ in the p_X^{LPS}, p_Y^{LPS} plane, where p_X^{LPS}, p_Y^{LPS} are the X and Y components of the proton momentum. Protons with $p_T^{LPS} \lesssim 0.2$ GeV and $x_L \simeq 1$ are too close to the beam to be safely measured. In the region covered by the LPS planes (200 MeV $\lesssim |p_X^{LPS}| \lesssim 400$ MeV, $|p_Y^{LPS}| \lesssim 600$ MeV) the acceptance is large, as shown by the lines in the figure: however, integrating over the azimuthal angle ϕ the resulting acceptance is $\simeq 6\%$. For $x_L > 0.97$ and $0.25 \lesssim p_T^{LPS} \lesssim 0.65$ GeV, the acceptance does not vary strongly with x_L and changes from 15% at low p_T^{LPS} to 2% at high p_T^{LPS}. The alignment uncertainty does not significantly affect the geometric acceptance, and, in this analysis, cuts were applied to ensure that the events lie in a well understood region.

6 Data selection

Deep inelastic events in the ZEUS detector were first selected online by a three-level trigger system (details can be found in [41]). At the first level DIS events were selected by requiring a minimum energy deposit in the electromagnetic section of the CAL. The threshold varied between 3.4 and 4.8 GeV depending on the position in the CAL. At the second level trigger, beam-gas background was reduced by using the measured times of energy deposits and the summed energies from the calorimeter. Events were accepted if $\delta = \sum_i E_i(1 - \cos \theta_i) > 24$ GeV $- 2E_\gamma$, where E_i, θ_i are the energies and polar angles of the calorimeter cells and E_γ is the energy measured in the luminosity photon calorimeter, thereby accounting for the photon emitted in events with initial state radiation. For fully contained events, the quantity δ is expected to be twice the positron beam energy, $\delta \simeq 55$ GeV. At the third level, algorithms to reject beam-halo and cosmic muons, as well as a stricter δ cut ($\delta > 25$ GeV $- 2E_\gamma$), were applied, together with the requirement of a scattered positron candidate with energy greater than 4 GeV.

Diffractive DIS candidate events were further selected offline in two steps: first the standard inclusive DIS selection was applied, then a high x_L track in the LPS was required.

Neutral current DIS events were selected as follows:

- A scattered positron with $E'_e > 10$ GeV was required, where E'_e is the energy after presampler correction with the SRTD (when available).

- The impact point of the scattered positron in the SRTD was required to be outside a square of 26×26 cm^2 centred on the beam. This cut ensures full containment of the positron shower in RCAL.

7

- $40 < \delta < 65$ GeV, to reduce the photoproduction background and the radiative corrections.

- The Z coordinate of the reconstructed vertex was required to be in the range $-50 < Z < 100$ cm.

- $y_e < 0.95$, where $y_e = 1 - E'_e(1 - \cos\theta_e)/2E_e$ is the value of y calculated from the positron variables (θ_e is the polar angle of the scattered positron).

- $y_{JB} > 0.03$, where $y_{JB} = \sum_h E_h(1 - \cos\theta_h)/2E_e$ is the value of y calculated from the hadronic energy flow [42]: in this case the combination of tracks and clusters described in section 4 was used.

The following cuts were applied to select diffractive events:

- A track in the LPS was required, with $0.97 < x_L < 1.01$, where the lower limit was applied to reduce non-pomeron exchange contributions and to select a region of uniform acceptance, while the upper limit corresponds to a $+2.5\sigma$ distance from the $x_L = 1$ peak, where σ is the average LPS resolution at $x_L \simeq 1$.

- The LPS track was extrapolated along the proton beam line. No track was accepted if, at any point, the minimum distance of approach to the beam pipe, Δ_{pipe}, was less than 500 μm. This cut reduces the sensitivity of the acceptance to the uncertainty in the position of the beam pipe apertures.

- The total $E + p_Z \simeq (E + p_Z)_{\mathrm{Cal}} + 2p_Z^{LPS} = \sum_i E_i(1 + \cos\theta_i) + 2p_Z^{LPS}$ of the event (the sum of the energy and the longitudinal component of the total momentum measured in the calorimeter and in the LPS) was required to be < 1655 GeV. For fully contained events this quantity should be equal to $2E_p = 1640$ GeV; the cut, which takes into account the resolution on the measured value of p_Z^{LPS}, reduces the background due to overlay events (see following section).

After this selection 553 events were left of which 376 were in the Q^2 region between 5 and 20 GeV^2.

Figures 2 to 4 show the distributions of the selected events and of the Monte Carlo model used in the analysis (weighted sum of the RAPGAP and the ρ^0 MC samples), as a function of Q^2, x, W, y_{JB} (figure 2), of $\eta_{max}, M_X, x_{I\!P}, \beta$ (figure 3) and of $x_L, |t|, p_X^{LPS}, p_Y^{LPS}$ (figure 4). The distributions are all uncorrected and the MC histograms are normalized to the number of events in the data; a cut of $Q^2 > 5$ GeV^2 was applied to both data and Monte Carlo samples. In fig. 3a, the variable η_{max} is the maximum pseudorapidity of all calorimeter clusters with an energy of at least 400 MeV or tracks with momentum of at least 400 MeV. In our previous analysis, events with a large rapidity gap were defined by $\eta_{max} \lesssim 1.5$-2.5 [4]: however the events with a tagged proton with $x_L > 0.97$ can have larger values of η_{max}. This allows us to study events with $M_X \gtrsim 20$ GeV, where the hadronic system extends close to the proton beam pipe, and no gap may be observed in the detector. In figs. 3c and 3d, the $\ln M_X^2$ distribution is shown in two W bins ($50 < W < 120$ GeV, $120 < W < 270$ GeV). The data and the diffractive MC model are in good agreement. Compared to our previous analyses, the data extend the explored kinematic region to higher values of M_X, and therefore to higher $x_{I\!P}$ and lower β.

8

7 Background

After the selection described in the previous section, the sample still contains some background, mainly due to beam-halo and DIS processes which are not single diffractive dissociation.

Proton beam-halo events originate from interactions of beam protons with the residual gas in the pipe or with the beam collimators. These events have a scattered proton of energy close to that of the beam: when they accidentally overlap with a genuine DIS event, they may give a false diffractive signal. Most of these events, however, appear to violate energy and momentum conservation. Figure 5 shows a scatter plot of x_L and the $(E + p_Z)_{\mathrm{Cal}}$ (measured with the calorimeter) for the DIS events selected in the LPS (excluding the x_L and the $E + p_Z$ cuts): a clear band at $x_L \simeq 1$, uncorrelated with the energy measured in the calorimeter, can be ascribed to beam-halo events. This type of background can be rejected by requiring that the total $E + p_Z$ of the event be conserved, as for beam-halo it can exceed the kinematic limit of 1640 GeV (see line in fig. 5). To evaluate the residual background after the cuts mentioned in the previous section, the $2p_Z^{LPS}$ distribution of events with unphysical tracks in the LPS ($(E + p_Z)_{\mathrm{Cal}} + 2p_Z^{LPS} > 1655$ GeV) was randomly mixed with the $(E + p_Z)_{\mathrm{Cal}}$ distribution for DIS events, to create a $E + p_Z$ distribution for beam-halo events. The obtained $E + p_Z$ distribution was normalized to the observed data distribution for $E + p_Z > 1655$ GeV. The remaining background (below the $E + p_Z = 1655$ GeV cut) was estimated to be less than 6%.

In order to evaluate the background due to proton dissociation and pion exchange, the cut on x_L was removed. Figure 6 shows the observed uncorrected x_L spectrum for the data (dots): a narrow diffractive peak is seen at $x_L \simeq 1$, together with a distribution at lower x_L due to the background processes mentioned above. Note that the acceptance falls by almost an order of magnitude between $x_L \simeq 0.8$ and $x_L \simeq 1$. These processes were modelled using the Monte Carlo programs described in section 5, EPSOFT for the proton dissociation, RAPGAP for the pion exchange, while for the diffractive signal the combined RAPGAP and ρ^0 MCs were used. The weighted sum of the three components was fitted to the observed x_L spectrum in the data in two steps. The weight factor for the proton dissociation events was first determined by normalizing the EPSOFT MC sample to the data in the region $x_L < 0.95$ and $\eta_{max} < 1.5$, where double dissociation dominates. The weight factors for the single diffraction and the pion exchange processes were determined by fitting the weighted sum of the three MC samples to the observed x_L distribution. The resulting sum is shown as the solid line in fig. 6. After applying the $x_L > 0.97$ cut, the background due to proton dissociation is less than 3%, to be compared with the 10-15% contamination estimated to be present in our previous analyses [4, 6]. The fit was repeated using different MC models (PYTHIA for proton dissociation, NZ plus ρ^0 for the signal) and consistent results were found. This estimate of the background due to proton dissociation was checked by looking at events tagged both in the proton remnant tagger PRT1 and in the LPS. According to simulations based on the EPSOFT Monte Carlo, the PRT1 has a tagging efficiency of approximately 50% for proton dissociation events; this leads, after the x_L cut, to an estimated contamination below 3%, consistent with the evaluation described above.

The background due to the pion exchange was found to be less than 1% after the $x_L > 0.97$ cut. Note that the fit to the x_L spectrum is used to give an estimate of the upper limit on the pion exchange background at high x_L and it is not meant to be a complete study of the distribution.

The background due to other reggeon exchanges was not included in this evaluation: at high $x_{I\!P}$ values ($x_{I\!P} \gtrsim 0.01$), a contribution from other reggeon exchanges is likely [5], however the predictions vary significantly in different models [43, 44]. The possible contribution of these additional trajectories at high $x_{I\!P}$ is discussed in section 9. Background due to non-diffractive DIS processes (not shown in the figure), in which one of the proton fragments is observed in the LPS, gives a contribution at small values of x_L.

The background due to non-ep interactions (excluding beam-halo events) was evaluated to be negligible from the data taken with the unpaired proton bunches. The background due to photoproduction events was found to be negligible from Monte Carlo studies.

As the backgrounds due to beam-halo, non-ep interactions, proton dissociation and pion exchange were found to be small compared with the statistical precision of the data, they were not subtracted in the results shown in the following.

8　Measurement of the t distribution

The measurement of the t dependence in diffractive DIS was limited to the kinematic range $0.073 < |t| < 0.4$ GeV^2, $5 < Q^2 < 20$ GeV^2, $50 < W < 270$ GeV, $0.015 < \beta < 0.5$ and $x_L > 0.97$. The range in $|t|$ was limited to values greater than 0.073 GeV^2, since for lower values of $|t|$ the acceptance varies rapidly; the upper limit of 0.4 GeV^2 restricts the data to a region where the LPS acceptance exceeds 2%. The bin widths in t were chosen to be larger than the resolution, resulting in four bins. The acceptance and the detector effects were unfolded using a bin-by-bin correction determined with the RAPGAP plus ρ^0 MC.

Figure 7 shows the measured differential cross section, $d\sigma/dt$. The distribution was fitted with a single exponential form, shown as the solid line:

$$d\sigma/dt = Ae^{bt}; \tag{9}$$

the value of the fitted parameter b is:

$$b = 7.2 \pm 1.1(\text{stat.})^{+0.7}_{-0.9}(\text{syst.}) \text{ GeV}^{-2}, \tag{10}$$

where the first uncertainty is statistical and the second is systematic.

The systematic uncertainties can be subdivided into three groups, those due to the DIS selection, those due to the LPS acceptance and background and, finally, those related to the unfolding. The systematic error due to the DIS acceptance was evaluated by changing the following cuts: the positron energy cut was moved to 8 GeV and 12 GeV, the cut on the impact position of the positron using the SRTD was moved to 24×24 cm^2 and to 28×28 cm^2; the y_{JB} cut was changed to 0.02 and 0.04. The effects on the slope b varied between $+5.5\%$ and -3%. To estimate the systematic contributions due to the LPS acceptance, the following checks were performed: the Δ_{pipe} cut was increased to 0.1 cm causing a negligible variation to the slope. The values of p_X^{LPS} and p_Y^{LPS} were shifted by ± 3 MeV and ± 6 MeV, respectively, as a test of the influence of the alignment procedure (see [24]), yielding variations on b between -6% and

$+3\%$. The mass M_X was reconstructed using the calorimeter for low masses and the LPS for high masses, giving changes around $\pm 5\%$ on the slope. The NZ plus ρ^0 Monte Carlo was used for the acceptance calculation, the t slope in RAPGAP was changed by ± 1 GeV^{-2}, the $\alpha'_{I\!P}$ value in the MC was changed from 0.25 GeV^{-2} to 0. These changes lead to variations of at most 4% for the slope b. The total systematic error was obtained by adding in quadrature the positive and negative deviations separately.

In a Regge-type approach [8], the slope of the exponential t distribution in single diffractive interactions is predicted to be $b \simeq b_0 + 2\alpha'_{I\!P} \ln(1/x_{I\!P})$. Assuming the value of $b_0 = 4.6$ GeV^{-2} inferred by Goulianos [45] from elastic $\bar{p}p$ scattering at $\sqrt{s} = 1800$ GeV [46] and $\alpha'_{I\!P} = 0.25$ GeV^{-2} [7], in the present kinematic range $(< x_{I\!P} > \simeq 8 \times 10^{-3})$ the measured b value is compatible with the predicted value of $\simeq 7$ GeV^{-2} for a soft pomeron exchange; it is also consistent with the values predicted by some perturbative QCD models [47].

9 Measurement of $F_2^{D(4)}$ and $F_2^{D(3)}$

The measurement of the proton in the LPS permits the determination of the cross section for single diffractive dissociation in DIS as a function of the four kinematic variables $\beta, Q^2, x_{I\!P}$ and t. Given the small statistics collected in the 1994 running, the measurement was performed in a single t bin, $0.073 < |t| < 0.4$ GeV^2 and a single Q^2 bin, $5 < Q^2 < 20$ GeV^2, with average values of $< |t| > = 0.17$ GeV^2 and $< Q^2 > = 8$ GeV^2. The sizes of the β and $x_{I\!P}$ bins were chosen to be larger than the resolutions (see section 4); a minimum number of 8 events in each bin was also required. The chosen bins are shown in figure 8: they are in the range $4 \times 10^{-4} < x_{I\!P} < 0.03, 0.015 < \beta < 0.5$. The acceptance, which includes the efficiency of the DIS selection and the geometric acceptance of the LPS, varies between 3% and 11% in these bins. The purity, defined as the ratio of the number of MC events generated in a bin and reconstructed in the same bin over the number of events reconstructed in that bin, was required to be greater than 25% in the bins used for the measurement and is typically more than 40%. The effect of the longitudinal structure function F_L is assumed to be smaller than the statistical errors in the kinematic range considered [4] and is neglected.

In order to extract the structure function $F_2^{D(4)}$, the weighted sum of the RAPGAP and the ρ^0 MC, which gives a good description of the data, was used to obtain the correction for acceptance with a bin-by-bin unfolding method. In addition a bin centring correction was applied, using the $F_2^{D(4)}$ parametrization of the RAPGAP MC.

The following systematic checks were performed for the measurement of $F_2^{D(4)}$:

- To check the photoproduction background and the QED radiative corrections, the cut on δ was changed to 37 GeV and 42 GeV, and the cut on the scattered positron energy was varied to 8 GeV and 12 GeV. The effect was typically up to 3%.

- To check the acceptance at low Q^2 which is determined by the positron position, the cut on the impact point of the positron was changed to 24×24 cm^2 and to 28×28 cm^2; both induced variations on $F_2^{D(4)}$ smaller than 15%.

11

- An alternative method to reconstruct the kinematics, the Σ method [48], was used, giving typical variations of about 20%.

- The cut on y_{JB} was moved by $\pm$ 0.01, yielding changes of typically around 10%.

- The cut on the minimum energy deposit of the EMC (HAC) cells was moved to 140 (160) MeV and to 80 (120) MeV, to check the effect of the calorimeter noise on the mass reconstruction. The effect was between 10% and 25% for the first cut, and up to 15% for the second check.

- The LPS track selection was modified by raising the Δ_{pipe} cut to 0.1 cm, producing variations of $F_2^{D(4)}$ of less than 12%.

- To check the background estimation due to one-pion exchange and proton dissociation, MC predictions were statistically subtracted from the bins, producing changes up to 5% in a few bins. The beam-halo was also subtracted with negligible effects on $F_2^{D(4)}$. The x_L cut was moved to 0.96, causing changes on $F_2^{D(4)}$ of less than 5%, except in one bin at high $x_{I\!P}$ where the change was 15%.

- An alternative method to reconstruct the mass M_X was employed, which uses $1.25 \cdot M_X^{meas}$ at low masses and M_X^{LPS} at high masses, giving an effect of less than 2% at high β and up to 25% at low β.

- An unfolding method based on Bayes' theorem [49] was applied for the acceptance correction causing variations typically less than 3%. The NZ plus ρ^0 Monte Carlo was used to unfold, giving changes typically less than 20%, except at low β where the changes were up to 40%. The $x_{I\!P}$ and t dependence in RAPGAP were reweighted to a fixed t dependence of the form $(1/x_{I\!P})e^{-7|t|}$ or to a fixed $x_{I\!P}$ dependence of the form $(1/x_{I\!P})^{1.3}$, yielding changes of less than 5%.

Most of the systematic checks yielded results which agree with the central value within the statistical errors. The negative and positive deviations in each bin were separately combined in quadrature.

The results for $F_2^{D(4)}$ are given in table 1. The systematic errors do not include a 5.5% overall normalization uncertainty due to the luminosity determination and trigger efficiency (2%) and due to the LPS acceptance varying because, due to the proton beam conditions, the LPS stations had to be positioned differently in different runs (5%). The values of $F_2^{D(4)}$ are plotted in fig. 9 as $x_{I\!P} \cdot F_2^{D(4)}$ as a function of $x_{I\!P}$, in four β intervals, with central values of $\beta = 0.028, 0.07, 0.175$ and 0.375, respectively. The $F_2^{D(4)}$ data are observed to fall rapidly with increasing $x_{I\!P}$. To investigate whether the $x_{I\!P}$ dependence is the same in all β intervals, we performed fits of the form:

$$F_2^{D(4)} = A_i \cdot (1/x_{I\!P})^a , \tag{11}$$

where the normalization constants A_i were allowed to vary in each bin, while the exponent a was constrained to be the same in all four β bins. The result of the fit is

$$a(0.073 < |t| < 0.4 \text{ GeV}^2) = 1.00 \pm 0.09 \text{ (stat.)}^{+0.11}_{-0.05}(\text{syst.}), \tag{12}$$

with a χ^2 value of 10 for 8 degrees of freedom, showing that the result is consistent with a single $x_{I\!P}$ dependence in all β bins. The systematic error was obtained by re-fitting the $F_2^{D(4)}$ values obtained for each of the systematic checks mentioned above. The main contributions arose from changing the unfolding procedure (4%), using the Σ method (5%) and applying different noise suppression cuts (7%).

In order to compare with previous measurements of the diffractive structure function, we extracted $F_2^{D(3)}(\beta, Q^2, x_{I\!P})$ by integrating $F_2^{D(4)}$ over t. The extrapolation to the whole t range $(0 < |t| < \infty)$ was performed using the $F_2^{D(4)}$ parametrization in the MC. The result is shown in table 1 and is plotted as $x_{I\!P} \cdot F_2^{D(3)}$ in figure 10. Fitting our data in each β interval with the form $(1/x_{I\!P})^{\overline{a}}$ yielded a value $\overline{a} = 1.01 \pm 0.10$ (stat.)$^{+0.11}_{-0.06}$(syst.).

This value of $\overline{a}$ is much lower than the value obtained with the ZEUS 1993 data [4], based on a large rapidity gap analysis[2]. The ZEUS 1993 $F_2^{D(3)}$ result corresponds to $0.1 < \beta < 0.8$ and $6.3 \times 10^{-4} < x_{I\!P} < 10^{-2}$, for $8 < Q^2 < 100$ GeV^2, and it is compatible with a single $x_{I\!P}$ dependence in all β bins, with slope $\overline{a} = 1.30 \pm 0.08$(stat.)$^{+0.08}_{-0.14}$(syst.). As already mentioned, the present analysis covers a different kinematic range, extending to lower β and higher $x_{I\!P}$ at $< Q^2 > = 8$ GeV^2. The lower value of $\overline{a}$ compared to our previous result may be ascribed to the presence of additional subleading trajectories contributing in the $x_{I\!P}$ range covered by this analysis. This contribution has been already observed in the analysis of the H1 1994 data [5], which are shown for comparison in fig. 10. Only the points at the Q^2 and β values closest to the ones presented here are shown. Assuming pomeron exchange to be the dominant contribution, the values of $a(0.073 < |t| < 0.4$ GeV$^2)$ and $\overline{a}$ can be related, respectively, to the $\alpha_{I\!P}$ value in the given t range and $\overline{\alpha_{I\!P}}$, the pomeron trajectory averaged over t (see section 2). However, as already mentioned in section 7, at high $x_{I\!P}$ a contribution from reggeon exchange cannot be excluded, in addition to pomeron exchange: the statistical precision of our data does not allow us to identify this component. As the reggeon trajectory has an intercept $\alpha_M \simeq 0.5$, leading to an $x_{I\!P}$ slope $a \simeq 0$, its presence would lower the expected $x_{I\!P}$ slope in the $x_{I\!P}$ region where the reggeon exchange contributes. The $x_{I\!P}$ range covered by this analysis could then explain the different result on the slope $\overline{a}$ compared to our previous result. Moreover, models where the pomeron component is not factorizable can lead to a different $x_{I\!P}$ slope parameter, depending on the kinematic range.

We have also examined the β dependence of the diffractive structure function. In order to do this, the $F_2^{D(3)}$ values within each β bin are plotted in figure 11, extrapolated to a common value of $x_{I\!P} = 0.01$, assuming a universal, fixed slope $\overline{a} = 1.01$. The solid line represents a fit of the form $b \cdot (1/x_{I\!P})^{\overline{a}} [\beta(1-\beta) + c/2(1-\beta)^2]$ to the measured $F_2^{D(3)}$. The values obtained in the fit are: $b = 0.087 \pm 0.015$ (stat.)$^{+0.014}_{-0.022}$(syst.) and $c = 0.34 \pm 0.11$ (stat.)$^{+0.25}_{-0.10}$(syst.). This fit to the present data indicates that both a hard $(\propto \beta(1-\beta))$ and a soft $(\propto (1-\beta)^2)$ component are needed. The parametrization obtained in our previous analysis [4], extrapolated to $x_{I\!P} = 0.01$ and scaled down by 15% to take into account the proton dissociation background contribution, is also shown in the figure as the dashed curve.

---

[2]We do not compare here to the result in ref. [6], as this result was affected by a technical error in the Monte Carlo generation used for the unfolding, which led to a higher $\overline{a}$ value by about one unit of the quoted error.

10 Conclusions

Diffractive DIS events have been studied at HERA using the ZEUS leading proton spectrometer. A clean sample of events was selected by requiring a scattered proton with $x_L > 0.97$. The background due to proton dissociation was estimated to be approximately 3%, substantially lower than in our previous analyses. The use of the LPS has also allowed an extension of the ZEUS measurements to values of the final state hadronic mass M_X as high as 35 GeV.

The t dependence was measured for the first time in this process in the range $0.073 < |t| < 0.4$ GeV^2, $5 < Q^2 < 20$ GeV^2, $0.015 < \beta < 0.5$ and $50 < W < 270$ GeV. The resulting distribution is described by the function e^{bt}, with $b = 7.2 \pm 1.1(\text{stat.})^{+0.7}_{-0.9}(\text{syst.})$ GeV^{-2}.

The diffractive structure function $F_2^{D(4)}(\beta, Q^2, x_{I\!P}, t)$ was measured in the interval $0.015 < \beta < 0.5$, $4 \times 10^{-4} < x_{I\!P} < 3 \times 10^{-2}$ and averaged over the range $0.073 < |t| < 0.4$ GeV^2 and $5 < Q^2 < 20$ GeV^2. Because of the limited statistical precision of the data, it is not possible to determine whether a different $x_{I\!P}$ dependence is needed in different $x_{I\!P}$ and β ranges. The $x_{I\!P}$ dependence is consistent, in all β intervals, with the form $(1/x_{I\!P})^a$, with $a(0.073 < |t| < 0.4$ GeV$^2) = 1.00 \pm 0.09$ (stat.)$^{+0.11}_{-0.05}$(syst.). Integrating over t, the structure function $F_2^{D(3)}$ was determined. A fit of the form $(1/x_{I\!P})^{\bar{a}}$ to $F_2^{D(3)}$ yielded $\bar{a} = 1.01 \pm 0.10$ (stat.)$^{+0.11}_{-0.06}$(syst.).

The result for the effective $x_{I\!P}$ slope is lower than that obtained in our previous measurement. This analysis, however, extends the $F_2^{D(3)}$ measurement to values of $x_{I\!P}$ up to 0.03, where a significant component of reggeon exchange could contribute to lowering the effective $x_{I\!P}$ slope parameter $\bar{a}$.

Acknowledgements

References

[1] ZEUS Collaboration, M. Derrick et al., Phys. Lett. B315 (1993) 481.

[2] H1 Collaboration, T. Ahmed et al., Nucl. Phys. B429 (1994) 477.

[3] H1 Collaboration, T. Ahmed et al., Phys. Lett. B348 (1995) 681.

[4] ZEUS Collaboration, M. Derrick et al., Z. Phys. C68 (1995) 569.

[5] H1 Collaboration, C. Adloff et al., DESY report DESY 97-158.

[6] ZEUS Collaboration, M. Derrick et al., Z. Phys. C70 (1996) 391.

[7] A. Donnachie and P.V. Landshoff, Nucl. Phys. B244 (1984) 322;
Phys. Lett. B296 (1992) 227.

[8] A.H. Mueller, Phys. Rev. D2 (1970) 2963; ibid. D4 (1971) 150;
D. Field and G. Fox, Nucl. Phys. B80 (1974) 367.

[9] For a review, see e.g. K. Goulianos, Phys. Rep. 101 (1983) 169.

[10] UA4 Collaboration, D. Bernard et al., Phys. Lett. B186 (1987) 227.

[11] UA8 Collaboration, R. Bonino et al., Phys. Lett. B211 (1988) 239;
UA8 Collaboration, A. Brandt et al., Phys. Lett. B297 (1992) 417.

[12] E710 Collaboration, N.A. Amos et al., Phys. Lett. B301 (1993) 313.

[13] CDF Collaboration, F. Abe et al., Phys. Rev. D50 (1994) 5535.

[14] E612 Collaboration, T.J. Chapin et al., Phys. Rev. D31 (1985) 17.

[15] H1 Collaboration, C. Adloff et al., Z. Phys. C74 (1997) 221.

[16] ZEUS Collaboration, J. Breitweg et al., Z. Phys. C75 (1997) 421.

[17] G. Ingelman and P. Schlein, Phys. Lett. B152 (1985) 256.

[18] ZEUS Collaboration, M. Derrick et al., Phys. Lett. B293 (1992) 465;
The ZEUS Detector, Status Report 1993, DESY 1993.

[19] A. Andresen et al., Nucl. Inst. Meth. A309 (1991) 101;
A. Caldwell et al., Nucl. Inst. Meth. A321 (1993) 356;
A. Bernstein et al., Nucl. Inst. Meth. A336 (1993) 23.

[20] C. Alvisi et al., Nucl. Inst. Meth. A305 (1991) 30.

[21] N. Harnew et al., Nucl. Inst. Meth. A279 (1989) 290;
B. Foster et al., Nucl. Phys. B (Proc. Suppl.) 32 (1993) 181;
B. Foster et al., Nucl. Inst. Meth. A338 (1994) 254.

[22] ZEUS Collaboration, M. Derrick et al., Z. Phys. C69 (1996) 607.

[23] J. Andruszkòw et al., DESY Report DESY 92-066;
ZEUS Collaboration, M. Derrick et al., Z. Phys. C63 (1994) 391.

[24] ZEUS Collaboration, M. Derrick et al., Z. Phys. C73 (1997) 253.

[25] U. Amaldi et al., Phys. Lett. B43 (1973) 231.

[26] S. Bentvelsen, J. Engelen and P. Kooijman, Proceedings of the Workshop "Physics at HERA", vol. 1, DESY (1992) 23.

[27] A. Abramowicz, A. Caldwell and R. Sinkus, Nucl. Inst. Meth. A365 (1995) 508.

[28] H. Jung, DESY Report DESY 93-182.

[29] K.H. Streng, in Proc. of the Workshop "Physics at HERA", p. 365, ed. R.D. Peccei (Hamburg 1987).

[30] K. Kwiatkowski, H. Spiesberger and H.-J. Möhring, Proceedings of the Workshop "Physics at HERA" vol. 3, DESY (1992) 1294.

[31] L. Lönnblad, Comp. Phys. Comm. 71 (1992) 15;
L. Lönnblad, Z. Phys. C65 (1995) 285.

[32] T. Sjöstrand and M. Bergtsson, Comp. Phys. Comm. 43 (1987) 367.

[33] ZEUS Collaboration, M. Derrick et al., Phys. Lett. B380 (1996) 220.

[34] N.N. Nikolaev and B.G. Zakharov, Z. Phys. C53 (1992) 331;
M. Genovese, N.N. Nikolaev and B.G. Zakharov, JETP 81 (1995) 625.

[35] A. Solano, Ph.D. Thesis, University of Torino 1993 (unpublished).

[36] ZEUS Collaboration, M. Derrick et al., Phys. Lett. B356 (1995) 601.

[37] M. Kasprzak, PhD thesis, Warsaw University (1996), DESY Internal Report F35D-96-16.

[38] H.-U. Bengtsson and T. Sjöstrand, Comp. Phys. Comm. 46 (1987) 43;
T. Sjöstrand, CERN TH-7112-93, (1994).

[39] L.L. Frankfurt, L. Mankiewics and M.I. Strikman, Z. Phys. A334 (1989) 343.

[40] GEANT 3.13, R. Brun et al., CERN DD/EE/84-1 (1987).

[41] ZEUS Collaboration, M. Derrick et al., Z. Phys. C72 (1996) 399.

[42] F. Jacquet and A. Blondel, Proceedings of "The study of an *ep* facility for Europe", DESY 79/48 (1979) 391.

[43] K. Golec-Biernat, J. Kwieciński and A. Szczurek, INP Cracow preprint 1754/PH, hep-ph/9701254.

[44] N.N. Nikolaev, W. Schäfer and B.G. Zakharov, preprint KFA-IKP(Th)-1996-06, hep-ph/9608338.

[45] K. Goulianos, Phys. Lett. B358 (1995) 379 (and Erratum in Phys. Lett. B363 (1995) 268).

[46] CDF Collaboration, F. Abe et al., Phys. Rev. D50 (1994) 5518.

[47] N.N. Nikolaev, B.G. Zakharov and V.R. Zoller, Phys. Lett. B366 (1996) 337.

[48] U. Bassler and G. Bernardi, Nucl. Inst. Meth. A361 (1995) 197.

[49] G. D'Agostini, Nucl. Inst. Meth. A362 (1995) 487.

β	x_{IP}	N_{obs}	$F_2^{D(4)} \pm stat. \pm sys.$ GeV^{-2}	$F_2^{D(3)} \pm stat. \pm sys.$
0.028	0.011	14	$2.8 \pm 0.8^{+1.2}_{-0.6}$	$1.3 \pm 0.4^{+0.6}_{-0.3}$
0.028	0.024	17	$2.2 \pm 0.6^{+1.0}_{-0.9}$	$1.0 \pm 0.3^{+0.5}_{-0.4}$
0.07	0.0044	13	$7.8 \pm 2.3^{+2.0}_{-2.1}$	$3.6 \pm 1.1^{+1.0}_{-1.0}$
0.07	0.011	22	$3.8 \pm 0.9^{+1.3}_{-1.4}$	$1.8 \pm 0.4^{+0.6}_{-0.7}$
0.07	0.024	13	$1.8 \pm 0.5^{+0.7}_{-0.3}$	$0.8 \pm 0.2^{+0.4}_{-0.1}$
0.175	0.0018	15	$28.4 \pm 7.7^{+13.7}_{-4.8}$	$13.4 \pm 3.6^{+6.5}_{-2.1}$
0.175	0.0044	21	$10.8 \pm 2.5^{+3.4}_{-1.7}$	$5.0 \pm 1.2^{+1.8}_{-0.9}$
0.175	0.011	22	$5.3 \pm 1.2^{+1.2}_{-1.4}$	$2.5 \pm 0.6^{+0.5}_{-0.6}$
0.175	0.024	13	$3.6 \pm 1.1^{+1.0}_{-1.7}$	$1.7 \pm 0.5^{+0.7}_{-0.7}$
0.375	0.0007	19	$89.1 \pm 21.7^{+14.3}_{-18.6}$	$42.7 \pm 10.4^{+6.5}_{-6.4}$
0.375	0.0018	32	$53.6 \pm 10.4^{+8.6}_{-11.2}$	$25.3 \pm 4.9^{+4.3}_{-4.6}$
0.375	0.0044	16	$10.4 \pm 2.7^{+1.8}_{-4.2}$	$4.9 \pm 1.3^{+0.9}_{-1.8}$
0.375	0.011	8	$3.9 \pm 1.4^{+2.2}_{-1.0}$	$1.8 \pm 0.7^{+1.0}_{-0.3}$

Table 1: Results on $F_2^{D(4)}$ and $F_2^{D(3)}$ using the ZEUS LPS 1994 data at $Q^2 = 8$ GeV^2. The $F_2^{D(4)}$ values are in the t interval $0.073 < |t| < 0.4$ GeV^2, the $F_2^{D(3)}$ values are in the t range $0 < |t| < \infty$. The overall normalization uncertainty of 5.5% is not included and no background is subtracted from the data.
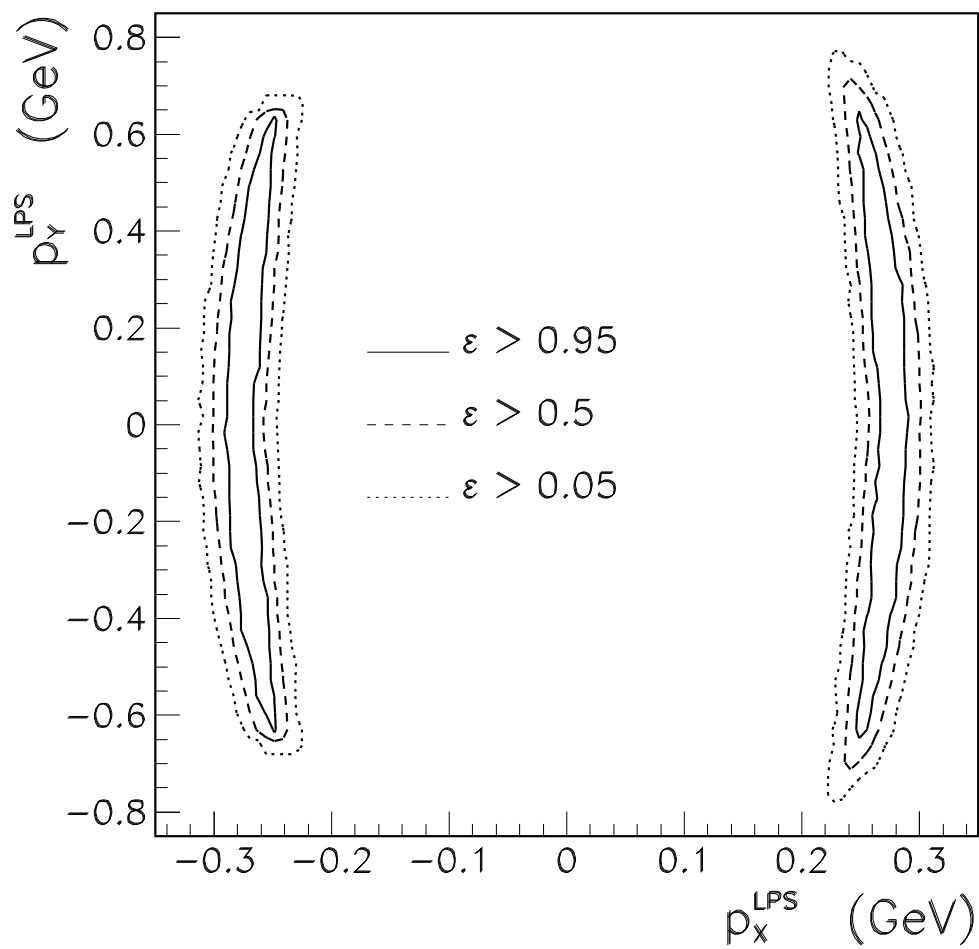
Figure 1: Geometric LPS acceptance for tracks with $x_L = 1$ in the p_X^{LPS}, p_Y^{LPS} plane. The lines indicate the regions where the acceptance is greater than $5\%, 50\%$ and 95%.
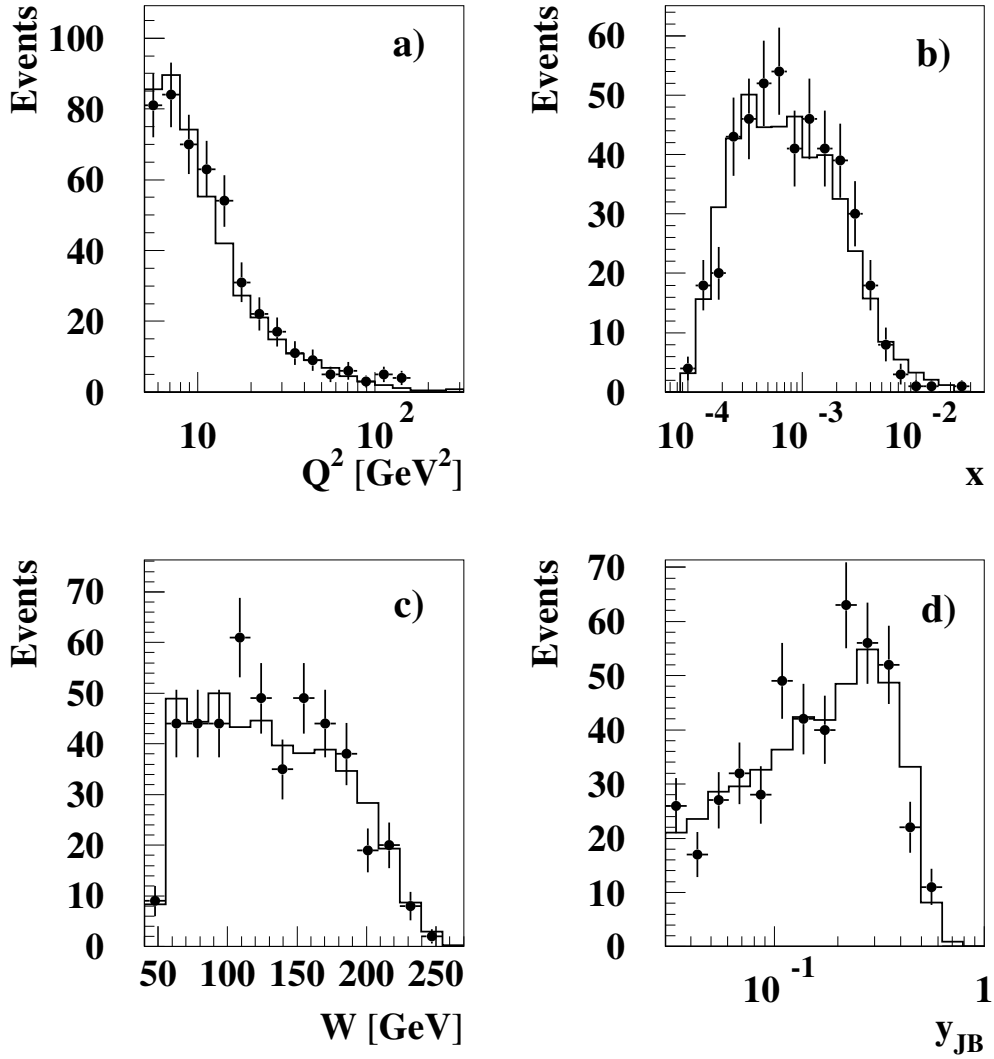
ZEUS 1994

Figure 2: Observed event distributions as a function of (a) Q^2, (b) x, (c) W, and (d) y_{JB} of the reconstructed data (dots) compared to the Monte Carlo model (solid line). The Monte Carlo is the weighted sum of the RAPGAP and ρ^0 samples. The errors, shown as vertical bars, are statistical only.
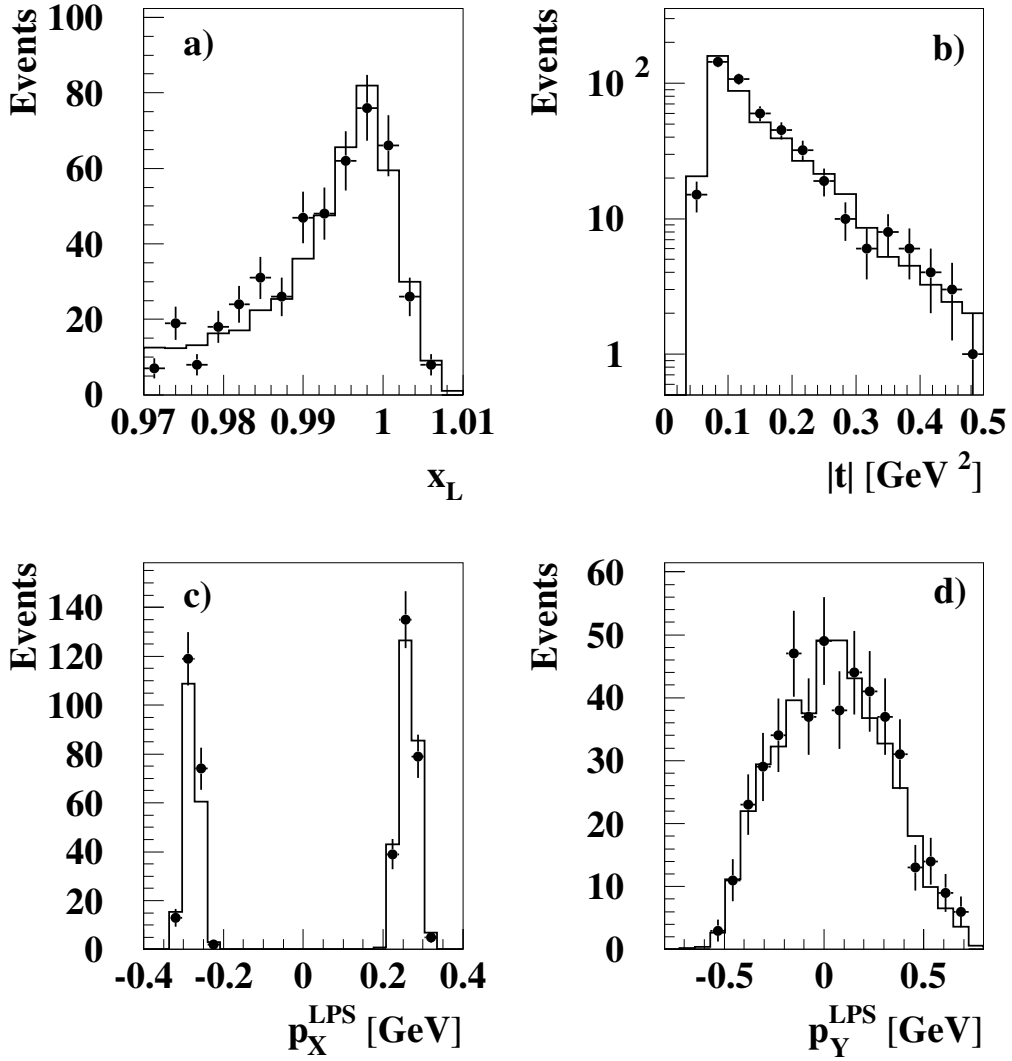
20

ZEUS 1994

Figure 3: Observed event distributions as a function of (a) η_{max} , (b) M_X, (c) $\ln M_X^2$ for $50 < W < 120$ GeV, (d) $\ln M_X^2$ for $120 < W < 270$ GeV, (e) $x_{I\!P}$ and (f) β of the reconstructed data (dots) compared to the Monte Carlo (solid line). The Monte Carlo is the weighted sum of the RAPGAP and ρ^0 samples. The errors are statistical only.
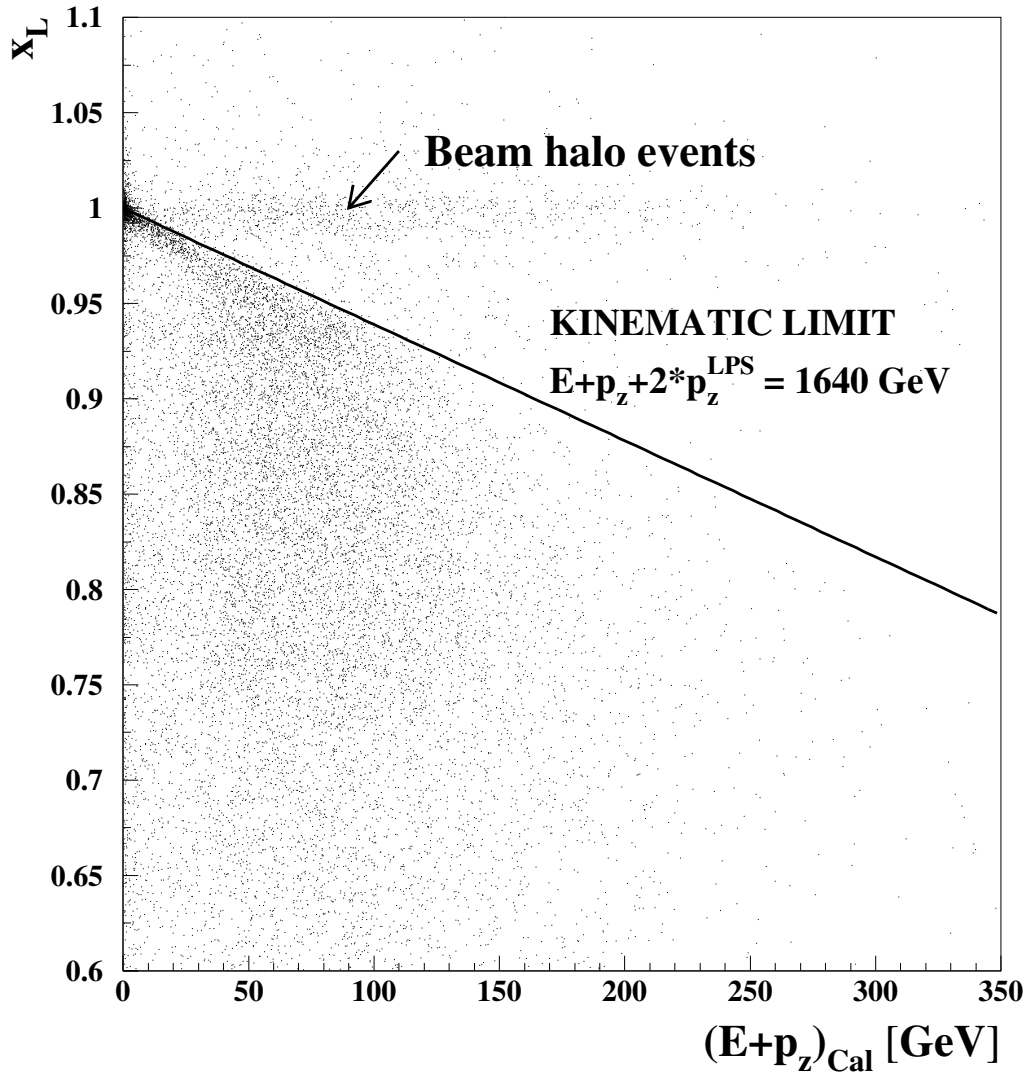
ZEUS 1994

Figure 4: Observed event distributions as a function of (a) x_L , (b) $|t|$, (c) p_X^{LPS} and (d) p_Y^{LPS} of the reconstructed data (dots) compared to the Monte Carlo (solid line). The Monte Carlo is the weighted sum of the RAPGAP and ρ^0 samples. The errors are statistical only.

Figure 5: A scatter plot of x_L and the $(E + p_Z)_{\mathrm{Cal}}$ as measured in the calorimeter in the data (before the x_L and the $E + P_Z$ cut). The region below the solid line indicates the allowed kinematic region.

ZEUS 1994
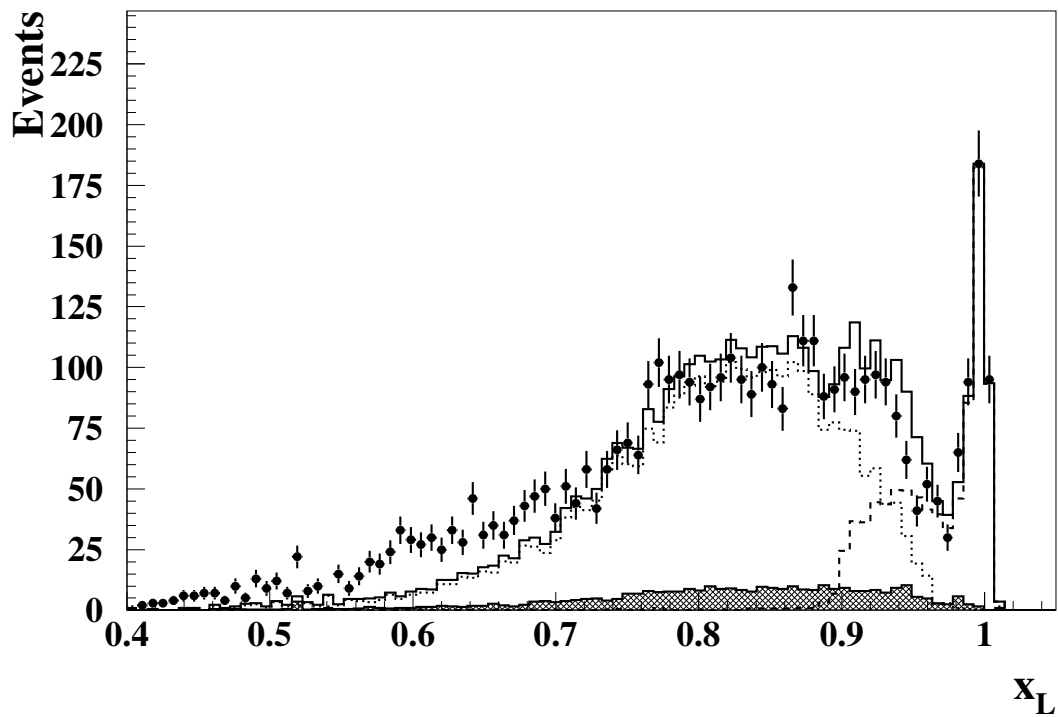
Figure 6: The observed x_L spectrum in the data (dots) where the x_L cut at 0.97 has been removed. Overlaid is the result of fitting the distribution with a sum (full line) of the contribution due to proton dissociation (EPSOFT MC – shaded area), of the maximum contribution due to pion exchange (dotted line) and of the single photon dissociation signal (RAPGAP plus ρ^0 MC – dashed line).
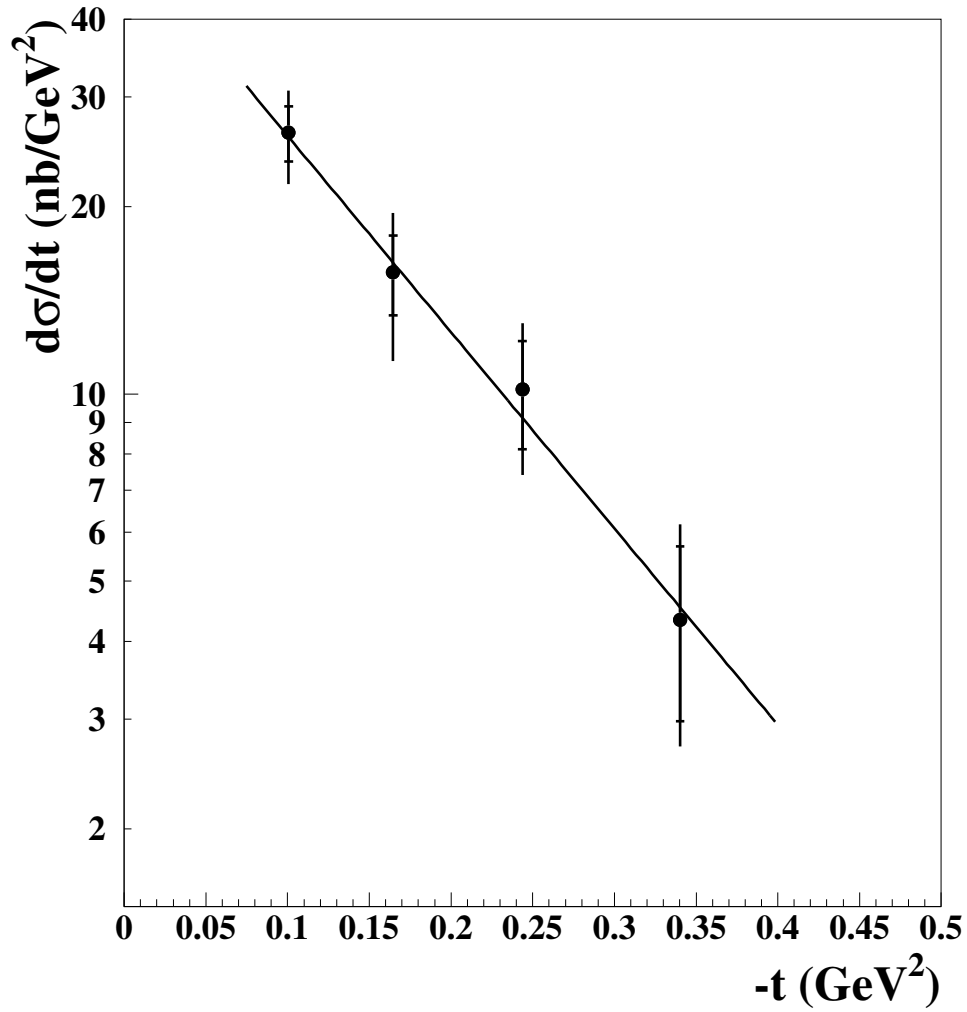
ZEUS 1994

Figure 7: The differential cross section $d\sigma/dt$ for diffractive DIS events with a leading proton of $x_L > 0.97$, in the range $5 < Q^2 < 20$ GeV^2, $50 < W < 270$ GeV and $0.015 < \beta < 0.5$. The inner error bars indicate the statistical errors, the outer error bars show the statistical and systematic errors added in quadrature. The line is the result of the fit described in the text.
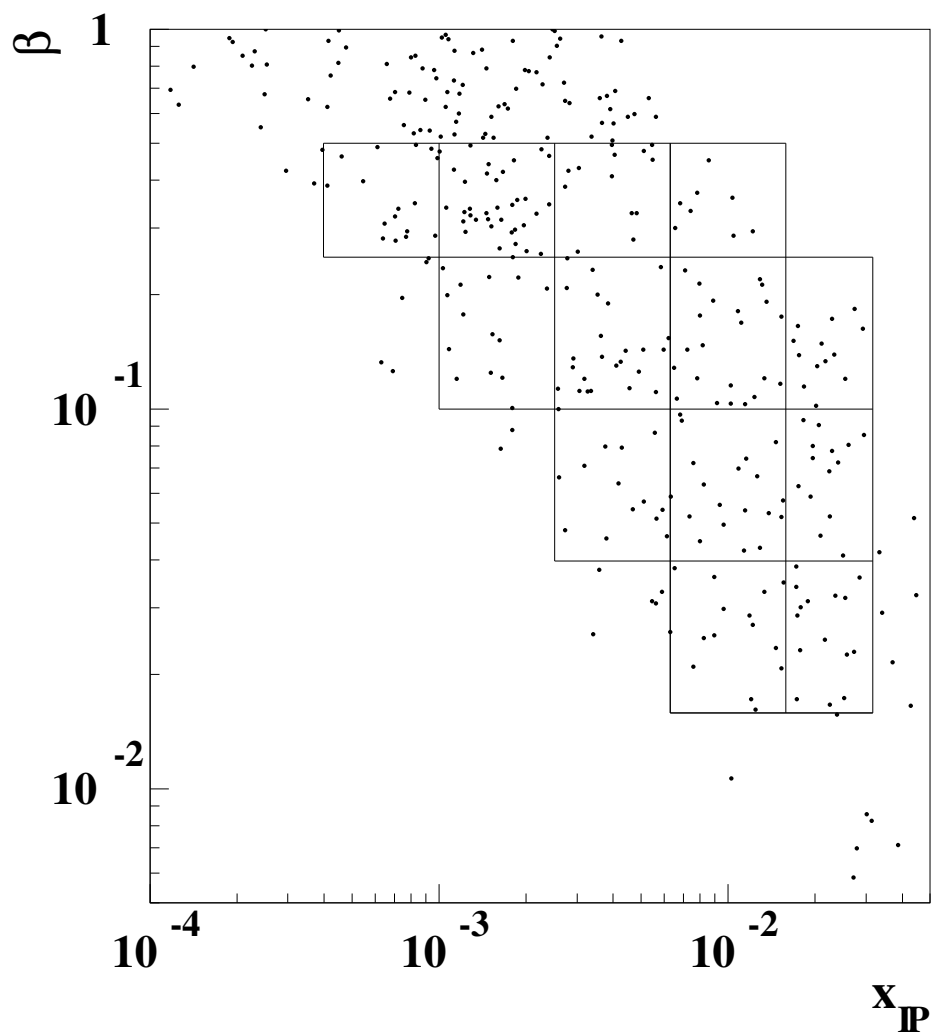
25

ZEUS 1994

Figure 8: The distribution of the events used in the analysis in the $\beta, x_{I\!P}$ plane. The bins in $\beta, x_{I\!P}$ used for the extraction of $F_2^{D(4)}$ and $F_2^{D(3)}$ are shown.
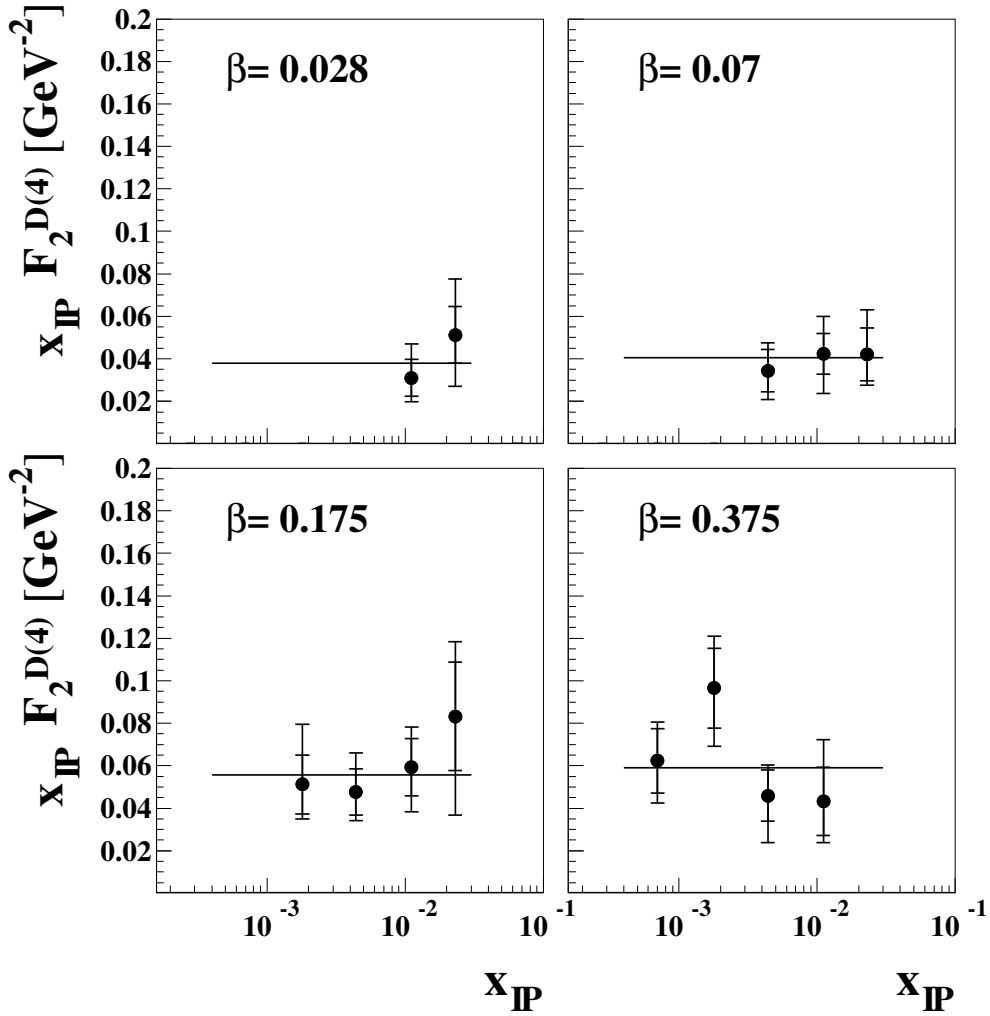
ZEUS 1994

Figure 9: The structure function $x_{I\!P} \cdot F_2^{D(4)}(\beta, Q^2, x_{I\!P}, t)$, plotted as a function of $x_{I\!P}$ in four β bins, at $< Q^2 > = 8$ GeV^2 and $< |t| > = 0.17$ GeV^2. The inner error bars indicate the statistical errors; the outer error bars are the sum of the statistical and systematic errors added in quadrature. The 5.5% normalization uncertainty is not included. The solid line corresponds to the fit described in the text.
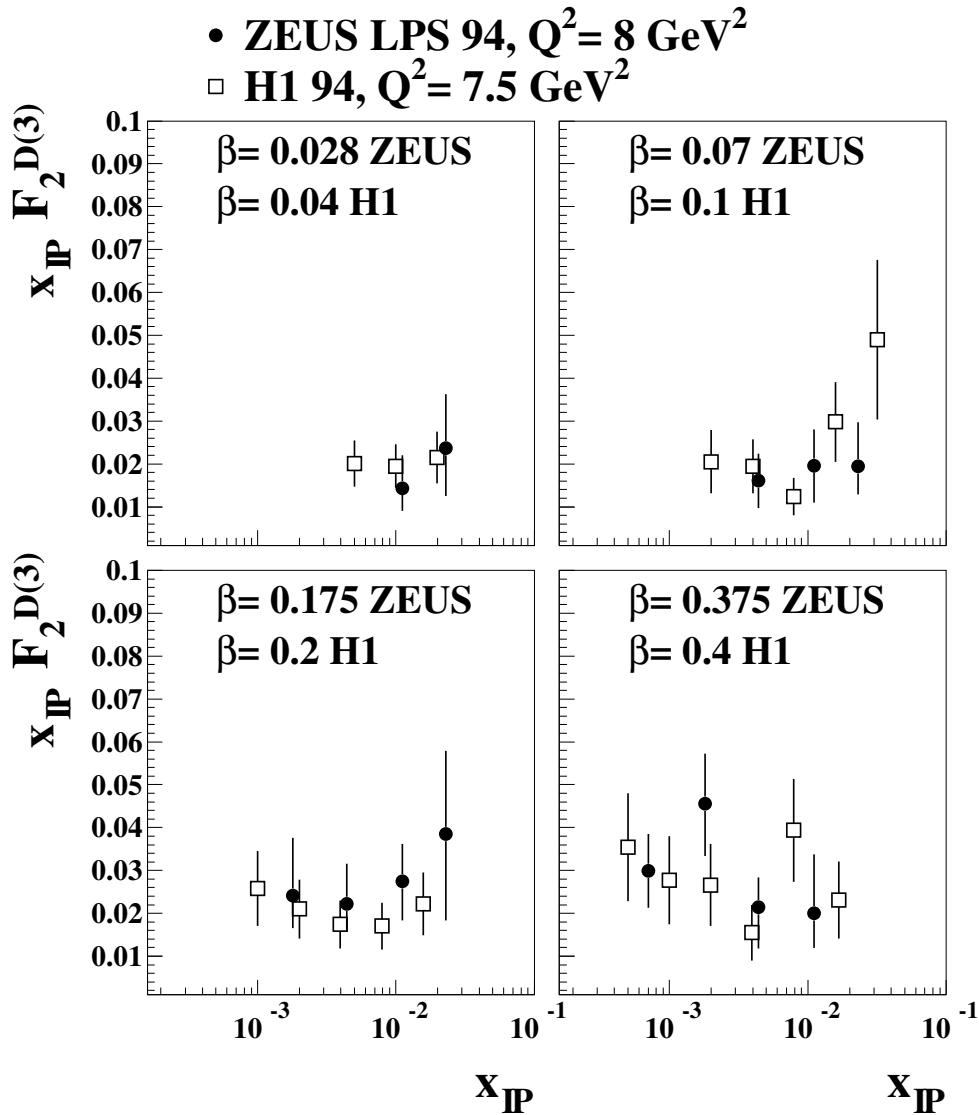
Figure 10: The function $x_{I\!P} \cdot F_2^{D(3)}(\beta, Q^2, x_{I\!P})$ for this analysis at $< Q^2 >= 8$ GeV² and $0 < |t| < \infty$, compared to the results at $< Q^2 >= 7.5$ GeV² and $|t| < 1$ GeV² from ref. [5]. The statistical and systematic errors are added in quadrature. The 5.5% and 6% normalization uncertainties of the ZEUS 1994 LPS data and of the H1 1994 data, respectively, are not included.
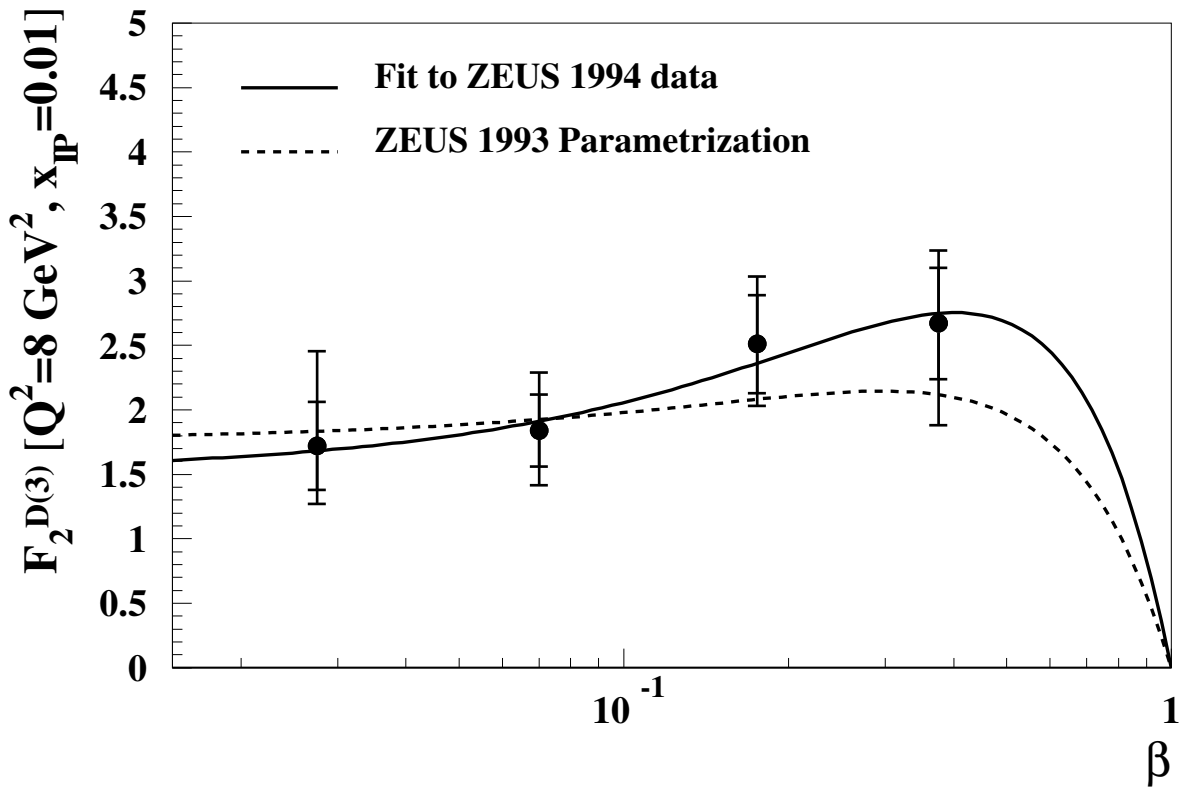
ZEUS 1994

Figure 11: The value of $F_2^{D(3)}(\beta, < Q^2 > = 8\ \mathrm{GeV}^2, x_{I\!P} = 0.01)$, obtained from the fits to the individual bins in β. The solid line represents the fit to the data as described in the text. The dashed line indicates the parameterization of ref. [4] scaled down to remove the estimated 15% double dissociative contributions.

29